

Optothermal characterization on thermal diffusivity, carrier diffusion and recombination properties of annealed thin Au film deposited on Si substrate

C. K. Sheng^{*}, M. G. M. Sabri, M. F. Hassan, E. A. G. E. Ali
*Faculty of Science and Marine Environment, Universiti Malaysia Terengganu,
21030 Kuala Nerus, Terengganu, Malaysia*

In this work, an optothermal wave characterization based on the photoacoustic (PA) technique was first implemented to investigate the thermal and carrier transport properties of Au thin film layer deposited on Si wafers (Au/Si) annealed at different temperatures. The XRD pattern showed that a metastable gold (Au) silicide of Au₈₁Si₁₉ phase formation was traced at annealing temperature of 330 °C and this structure disappeared when the temperature was further elevated up to 370 °C. The result showed that the PA signal obtained for Au/Si structure was lower than the pure Si wafer. The thermal and carrier transport properties of Si and Au/Si were elucidated from the fitting of PA signal-phase relation. From the result, the thermal diffusivity and surface recombination velocity of Au/Si increased with shorter recombination lifetime as the raise of annealing temperature. Nonetheless, as the temperature approaches 370 °C, the surface recombination and thermal transport process diminishes, which may be ascribed to the rupture of silicide clusters.

(Received July 20, 2021; Accepted October 29, 2021)

Keywords: Au silicide, Thermal annealing, Photoacoustic, Thermal diffusivity, Recombination

1. Introduction

New functionalities and applications of Si-based devices for greater performance can be achieved by using different surface modifications and treatments such as wet or dry etching, polymer or metal deposition on the Si substrates. Recently, metal silicide thin films formed by interaction of silicon with refractory and noble metals are widely applied as integral parts in nano- and microelectronics components, such as ohmic contacts, Schottky barriers, gate electrodes, local interconnects, and diffusion barriers. These essential applications are due to their low electrical resistivity and contact resistance to silicon with flexible process compatibility. Also, the silicide-silicon interface is free of surface imperfections and contaminations that leads to the most reliable and reproducible physical properties for electronics applications [1-6]. Optothermal-wave physics has become a well-defined and valuable tool in the study of materials thermo-optical parameters as well as in the semiconductor industry for characterizing processes in the electronic devices manufacturing. The optoacoustic or photoacoustic (PA) is one of the photothermal phenomena that based on the absorption of light by a sample enclosed in an airtight PA cell. The light absorbed by the sample is then converted into heat and as a result, the pressure fluctuation produced in the air chamber oscillates with the chopping frequency and is eventually detected as PA signal by a sensitive microphone coupled to the cell [7-12]. In the PA characterization, the heat generated from the conversion of sample light absorption depends mainly on the carrier transport properties of the semiconductor that involves non-radiative relaxation processes. Hence, three instantaneous heating sources in semiconductors are well- identified: The first one is due to intra-band non-radiative thermalization, which arises from the electron-phonon collisions within the conduction band (diffusion contribution). The second and third ones come from the non-radiative electron-hole pairs recombination in the bulk and at the surface, respectively. In this paper, we investigated the carrier transport properties (i.e carrier diffusion coefficient, surface recombination velocity, and bulk recombination time) and thermal diffusivity of Si and Au deposited Si substrate (Au/Si)

^{*} Corresponding author: chankoksheng@umt.edu.my

annealed at different temperatures. The measurement has been carried out by using the open photoacoustic cell (OPC) configuration at room temperature [13-15].

The mathematical expression for the PA signal generated in semiconductor has been validated by resorting to the thermal-piston model of Rosencwaig and Gersho (R-G) [16], under consideration of the above-mentioned heating sources. It has been found that for optically opaque semiconductor, the phase angle ϕ of the PA signal in the transmission configuration is given as follows by Neto et al. [17]

$$\tan(\Delta\phi) = \frac{(aD/\nu)(\omega\tau_{\text{eff}} + 1)}{(aD/\nu)(1 - \omega\tau_{\text{eff}}) - 1 - (\omega\tau_{\text{eff}})} \quad (1)$$

with $\tau_{\text{eff}} = \tau[(D/\alpha_s)-1]$ and $a = (\pi f / \alpha_s)^{1/2}$. Equation (4) is the formula used in this paper for data fitting purpose, where D represents the carrier diffusion coefficient (cm^2/s), ν denotes the surface recombination velocity (cm/s), α_s is the thermal diffusivity (cm^2/s) and τ_{eff} is the effective recombination lifetime and τ is the surface recombination lifetime [15-17].

2. Materials, preparation and characterizations

The substrate used in the present investigation was a p-type boron-doped Si (100) single crystal semiconductor wafer at a concentration of $1.5 \times 10^{14} \text{ cm}^{-3}$ with 10-20 Ωcm resistivity. The thickness of the substrate was measured to be 688 μm . It was cut into the square dimension of $(2 \times 2) \text{ cm}^2$. The substrates were pre-cleaned by washing with acetone and distilled water via solvent degreasing method [18]. Au thin films with thickness of 45 nm were deposited on the Si substrates at room temperature in argon gas (5.5 kV, 50 mA) by DC sputtering technique, model E5100 advanced sputter coater. The pressure in the chamber during sputtering was maintained at around 0.02-0.03 Torr. The Au deposited Si substrates were then annealed in an oven at various temperatures of 330 $^\circ\text{C}$, 350 $^\circ\text{C}$ and 370 $^\circ\text{C}$ for 30 min heating duration.

The PA signal was obtained by utilizing the open photoacoustic cell (OPC) technique. The OPC construction is schematically shown in Fig. 1. The microphone used was a small electret condenser type (Cirkit product, UK) that fixed to an aluminum chamber. The typical design of the microphone consists of a metallized electret diaphragm and metal back plate separated from the diaphragm by an air gap. The front air chamber adjacent to the metallized diaphragm is roughly 1.6 mm long. The back-plate acts as another electrode of the microphone. The electrodes were connected through a resistor and then directly connected to a preamplifier. The sample was located on the top of the circular hole of the OPC by employing the silicone grease. When the modulated He-Ne laser light (75 mW, $\lambda = 632.8 \text{ nm}$) illuminated onto the sample, the heat generated in the sample diffused to the air in the PA chamber. The periodic pressure wave in the chamber would then induce the diaphragm to oscillate and in turn to generate a voltage across the resistor of the microphone. Lastly, the resulted PA signal is amplified by a preamplifier and further analyzed using a lock-in amplifier (SR530). The formation of Au silicide was confirmed by Philips X-ray diffractometer (7602 EA Almelo).

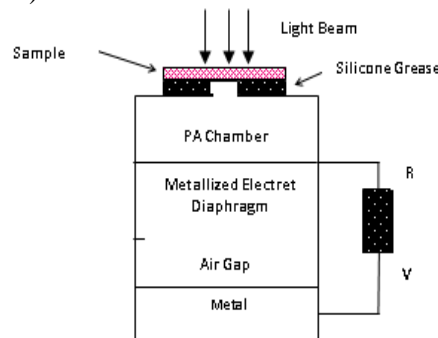


Fig. 1. Schematic cross section of the open photoacoustic cell detection.

3. Results and discussion

Fig. 2 displays the XRD pattern for the Si and Au/Si structure annealed at different temperatures of 300 °C, 350 °C and 370 °C. From the figure, a dominant sharp peak located at 69.3° denotes the (100) crystal plane of the Si substrate. This is the only peak observed on the XRD pattern that represents the single crystalline Si. Since the portion of Si is much higher than the other compounds, hence the peak of Si is highly intense and predominant than the others, causing those peak intensities are much smaller than Si, as can be visualized from the XRD diffractogram. Furthermore, the peak observed at 38.2° corresponds to Au (111) plane, showing that the Au deposited layer grows mainly in the [111] crystallite orientation. Meanwhile, a small peak positioned at 32.5° is ascribed to $\text{Au}_{81}\text{Si}_{19}$ mono-silicide structure at (200) plane, since only one unique peak that designates this silicide type appeared in the XRD pattern. From this result, it is worth to conjecture that the silicide begins to grow at 330 °C at the Si-Au interface, in which a minor peak that related to this phase is detected at this temperature. As the annealing temperature increases up to 350 °C, it can be clearly seen that the corresponding peak intensity increases, which might elucidate the formation of thicker aggregated $\text{Au}_{81}\text{Si}_{19}$ silicide accompanied with a larger surface area growth [6, 19, 20]. This effect is customarily associated to the annealing of Au/Si at a temperature that is slightly below and closer to bulk eutectic temperature of about 360 °C [19, 20]. Additionally, according to the previously reported work by Keum et al. [21], annealing at a temperature slightly above the bulk eutectic of Au/Si for less than 30 min could provide an excellent electrical contact with smooth Au film morphology. Moreover, in the present finding, the $\text{Au}_{81}\text{Si}_{19}$ silicide phase is found to disappear completely when the annealing temperature raises up to 370 °C. This is because the as-deposited Au thin film becomes ruptured at higher annealing temperature as evidenced by intensity reduction of Au peak, and hence resulting a weak bonding strength subsided between the Au/Si interfacial layers.

Fig. 3 illustrates the PA signal amplitude as a function of the modulation frequency for the pure Si and annealed Au/Si samples. The result shows that the PA signal decays when the modulation frequency increases. As the light beam is more frequently modulated at higher modulation frequency, causing the optical beam is not allowed to penetrate deeply into the samples, hence less heat is generated and transmitted to the gas medium before another heat pulse begins. As a consequence, the heat is mainly generated from the sample surface at higher frequency, which becomes essential to study the properties of a very thin film layer deposited on the substrates. Furthermore, it can be clearly seen from the figure that the PA signal intensity of Au deposited Si substrates is found lower than that of the pure Si substrate. This phenomenon might be explained by the reflection and light scattering effect from the Au/Si surface as compared to the smoother pure Si. On the other hand, the PA signal of Au/Si annealed at 330 °C and 350 °C is determined to be much lower than that of the sample annealed at 370 °C. This effect can be attributed to a greater bonding strength produced between the Au and silicide interfaces during the annealing process that eventually enhances the photon scattering of grain boundary [19].

Detailed analysis on the frequency dependence of PA signal phase data is customarily performed in order to obtain the thermal and carrier transport parameters of the current materials. According to Hernandez-Aguilar et al. [8], the PA signal phase is highly sensitive to the variation of carrier transport and recombination efficiency in the semiconductors. In the present work, the signal phase as a function of modulation frequency is presented in Fig. 4. From the figure, the observed nonlinear decay of the signal phase represents the intra-band non-radiative thermalization and recombination process of the photogenerated carriers, despite the same phenomenon is also reported in the literature [22]. Subsequently, by applying equation (4), curve fitting is performed on the signal phase data in the frequency range of 100 to 400 Hz, by letting D , v , α and τ as adjustable parameters. The best phase fitting of equation (4) to the phase data is represented by the solid lines. It can be clearly visible from the figure that the theoretical model is in good agreement with the experimental result, which reflects the validity of our approach.

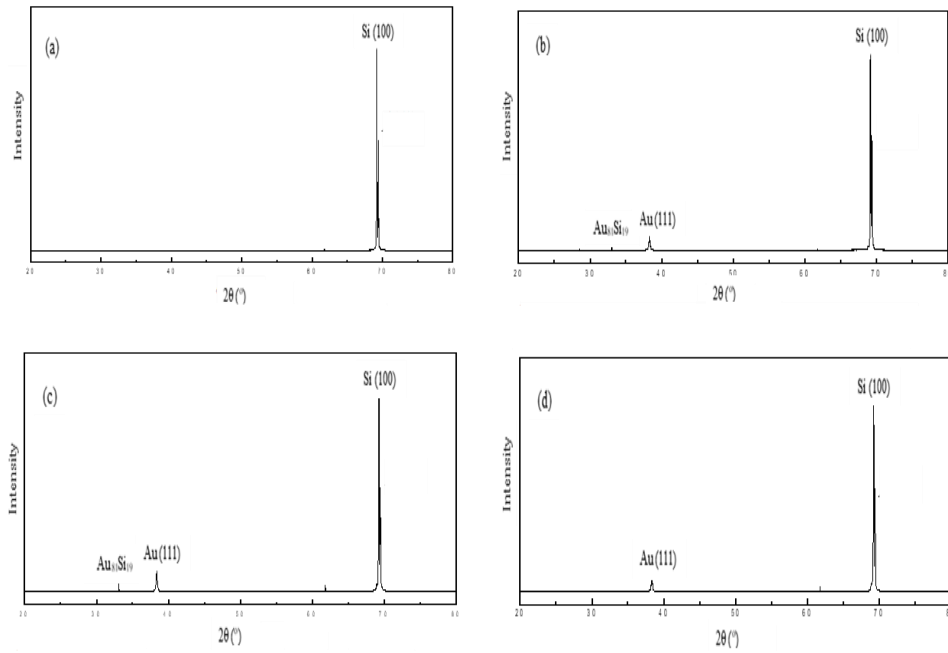


Fig. 2. The XRD patterns for (a) Si substrate and Au/Si prepared at various annealing temperatures of: (b) 330 °C, (c) 350 °C and (d) 370 °C.

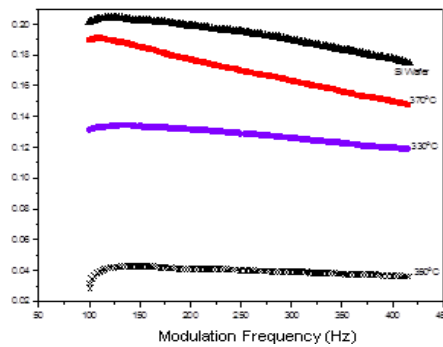


Fig. 3. PA signal amplitude versus modulation frequency for the Au/Si samples annealed at different temperatures.

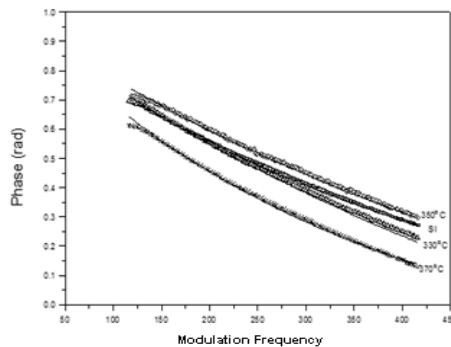


Fig. 4. Signal phase versus modulation frequency for the Si and Au/Si samples annealed at various temperatures.

In this work, the obtained parameter values of diffusion coefficient, thermal diffusivity, surface recombination velocity and recombination lifetime for the Au/Si samples annealed at different temperatures are summarized in Table 1. The fitted values of carrier diffusion coefficient for the Si substrate and all the Au/Si samples annealed at various temperatures are acquired to be 4.98 and 5.02 cm²/s, respectively. From this result, the diffusion coefficient of Au/Si is slightly higher than Si substrate, which might be due to the increased conducting efficiency of the carrier diffusion as contributed by the Au near Au/Si interface. Moreover, the result also indicates that the diffusion coefficient shows no dependence on the annealing temperature for the Au/Si samples within the studied.

Table 1. Parameter values of diffusion coefficient, thermal diffusivity, surface recombination velocity and recombination lifetime for the Au/Si samples annealed at different temperatures.

Sample	Thermal diffusivity (cm ² /s)	Diffusion coefficient (cm ² /s)	Surface recombination velocity (cm/s)	Recombination lifetime (μs)
p-type Si	1.020	4.98	322.2	15.42
Au/Si annealed at 330°C	1.030	5.02	329.1	10.23
Au/Si annealed at 350°C	1.070	5.02	335.0	11.05
Au/Si annealed at 370°C	0.908	5.02	303.7	15.35

Furthermore, the thermal diffusivity and surface recombination velocity increases as the annealing temperature elevated up to 350 °C. This tendency can be associated to the growth of eutectic Au₈₁Si₁₉ alloy that initiates an efficient carrier transference and electron-hole recombination processes across the surface and through the interface, since the Au or Au/Si possesses higher conductivity as compared to Si [23, 24]. Meanwhile, the band-to-band recombination lifetime of Au/Si annealed at 330 °C and 350 °C is determined lower than that of Si substrate. Such reduction in recombination lifetime dictates a faster recombination process occurred in the semiconductor materials [25]. Thus, it is interesting to note that once the Si surface was deposited by Au and annealed at a temperature close to the eutectic point, the surface recombination process increases, whereby more excess carriers are generated and recombined efficiently at a faster rate due to the formation of wider-area and thicker silicide clusters at Au/Si interface [6, 20]. Nevertheless, when the temperature increases up to 370 °C, the surface recombination and thermal transport diminishes. This phenomenon may be due to the fracture of the Au₈₁Si₁₉ silicide phase as validated by XRD analysis.

4. Conclusion

In summary, we have successfully characterized the thermal diffusivity, carrier diffusion and recombination properties Si substrate and Au/Si annealed at different temperatures using the PA optothermal-wave technique. A shorter band to band recombination lifetime accompanied with higher surface recombination velocity and thermal diffusivity of Au/Si are determined as compared to pure Si substrate and also for the Au/Si structure when annealed at elevated annealing temperature. The XRD pattern shows the formation of Au₈₁Si₁₉ monosilicide phase at temperature close to eutectic point and this structure rupture at higher annealing temperature of 370 °C.

Acknowledgements

The authors gratefully acknowledge the Faculty of Science and Marine Environment, UMT and Malaysian Government for the help in providing the research facilities, data and technical assistance in this work.

References

- [1] F. Nurhaziqah., C. K. Sheng, K. A. M. Amin, M. I. N. Isa, M. F. Hassan, E. A. G. E. Ali, K. H. Kamarudin, R. Aarif, ASM Science Journal Special Issue **1**, 68 (2018).
- [2] C. K. Sheng, T. J. E. Dwight, Results in Physics **10**, 5 (2018).
- [3] L. J. Chen, JOM **57**, 24 (2005).
- [4] V. D. Vankar, Proceedings of the Indian National Science Academy **57**, 195 (1991).
- [5] A. Gapska, M. Łapiński, P. Syty, W. Sadowski, J. E. Sienkiewicz, B. Kościelska, Beilstein Journal of Nanotechnology **9**, 2599 (2018).
- [6] N. Ye, J. P. Feser, S. Sadasivam, T. S. Fisher, T. Wang, C. Ni, A. Janotti, Physical Review B **95**, 085430 (2017).
- [7] C. K. Sheng, W. M. M. Yunus, W. M. Z. W. Yunus, Z. A. Talib, A. Kassim, Physica B: Condensed Matter **403**, 2634 (2008).
- [8] C. Hernandez-Aguilar, A. Dominguez-Pacheco, A. Cruz-Orea, R. Ivanov, Journal of Spectroscopy **2019**, 5920948 (2019).
- [9] O. E. Bonilla-Manrique, J. E. Posada-Roman, J. A. Garcia-Souto, M. Ruiz-Llata, Sensors **19**, 2890 (2019).
- [10] C. K. Sheng, W. M. M. Yunus, W. M. Z. W. Yunus, Z. A. Talib, A. Kassim, Solid State Science and Technology **15**, 16 (2007).
- [11] K. Dubyk, A. Pastushenko, T. Nychyporuk, R. Burbelo, M. Isaieva, V. Lysenko, Journal of Physics and Chemistry of Solids **126**, 267 (2019).
- [12] W. M. M. Yunus, C. K. Sheng, W. M. Z. W. Yunus, Journal of Nonlinear Optical Physics & Materials **12**, 91 (2003).
- [13] I. Delgadillo, M. Vargas, A. Cruz-Orea, J. J. Alvarado, Gil, R. Baquero, F. Sánchez-Sinencio, H. Vargas, Applied Physics B **64**, 97 (1996).
- [14] E. Marín, J. L. Pichardo, A. Cruz-Orea, P. Díaz, G. Torres-Delgado, I. Delgadillo, J. J. Alvarado-Gil, J. G. Mendoza-Alvarez, H. Vargas, Journal of Physics D: Applied Physics **29**, 981 (1996).
- [15] D. M. Todorovic, P. M. Nikolic, M. D. Dramicanin, D. G. Vasiljevic, Z. D. Ristovski, Journal of Applied Physics **78**, 5750 (1995).
- [16] A. Rosencwaig, A. Gersho, Journal of Applied Physics **47**, 64 (1976).
- [17] A. P. Neto, H. Vargas, N. F. Leite, L. C. M. Miranda, 1990. Physical Review B **40**, 3924 (1990).
- [18] T. J. E. Dwight, C. K. Sheng, M. I. N. Isa, Malaysian Journal of Analytical Sciences **15**, 227 (2011).
- [19] S. Chakraborty, J. Kamila, B. Rout, B. Satpati, P.V. Satyam, B. Sundaravel, B. N. Dev, Surface Science **54**, 149 (2004).
- [20] M. Sivakumar, K. Venkatakrishnan, B. Tan, Nanoscale Research Letters **6**, 78 (2011).
- [21] H. Keum, H. Chung, S. Kim, ACS Apply Materials and Interfaces **5**, 6051 (2013).
- [22] A. Barbu, G. Cristea, I. Bratu, V.P. Mushinskii, I. Bobis. Journal of Molecular Structure **410-411**, 259 (1997).
- [23] T. F. Young, J. F. Chang, H. Y. Ueng, Thin Solid Films **322**, 319 (1998).
- [24] C. K. Sheng, R. Aarif, E. A. G. E. Ali, M. F. Hassan, Journal of Sustainability Science and Management **15**(2), 6 (2020).
- [25] M. Kumar, S. Singh, P. K. Tiwari, S. H. Park, Digest Journal of Nanomaterials and Biostructures **15**(1), 75 (2020).